

HIGH PRECISION Al-Mg ISOTOPE STUDIES OF CONDENSATE CAIs. G. J. MacPherson¹, E. S. Bullock¹, P. E. Janney², A. M. Davis³, M. Wadhwa², and A. N. Krot⁴, ¹Department of Mineral Sciences, Museum of Natural History, Smithsonian Institution, Washington, DC 20560 USA macphers@si.edu. ²School of Earth & Space Exploration & Center for Meteorite Studies, Arizona State University, Tempe, AZ 85287. ³Department of the Geophysical Sciences & Enrico Fermi Institute, University of Chicago, Chicago, IL 60637. ⁴Hawai'i Institute of Geophysics and Planetology, University of Hawai'i at Manoa, Honolulu, HI 96822.

Introduction: A 1995 comprehensive review [1] of available Al-Mg isotopic data for Ca-Al-rich inclusions (CAIs) concluded that the initial $^{26}\text{Al}/^{27}\text{Al}$ ratio at the time of solar system formation was $\sim 4.5 \times 10^{-5}$. The data cited in that study were largely obtained by ion microprobe (without multicollection) and hence subject to rather large uncertainties by current standards. Recently, several studies have used far more precise multicollector ICPMS techniques to examine the Al-Mg isotopic systematics in bulk CAIs and in individual minerals within CAIs [2-4]. These studies suggest a higher initial ratio, $(^{26}\text{Al}/^{27}\text{Al})_0 \sim 6 \times 10^{-5}$ at the time of Al-Mg chemical fractionation, which is presumed to be the formation of CAI precursors by nebular condensation. The value of 4.5×10^{-5} would thus reflect the later time of final CAI formation. In fact, all of these high precision data came from inclusions that were either melted or at least heavily recrystallized early in their history. Therefore, a clear test of this hypothesis is to measure high-precision Al-Mg isotopic data on inclusions that not only have not been melted but that also bear the unmistakable chemical and textural imprints of actual condensation. This study presents data for 3 spinel-rich, fine-grained CAIs from CV3 chondrites that are all known to have volatility-fractionated trace element patterns (Group II) that can only be explained by condensation [5,6].

Samples: Chips of two CAIs from Allende (USNM #s 3529-40, 3529-43) and one from Leoville (USNM 3536-1) were prepared into polished thick mounts and photographed via backscattered electron (b.s.e.) imaging. Trace elements and descriptions of these CAIs (all \sim cm-sized) were previously reported [7-9]. Allende 3529-40 is notable for the abundance of hibonite (Fig. 1) that in places is concentrated into nearly monomineralic clumps; other abundant phases are Fe-rich spinel, aluminous diopside, nepheline and sodalite. Allende 3529-43 contains large (50-100 μm) patches of nearly monomineralic nepheline and (separately) sodalite, in addition to abundant aluminous diopside and Fe-bearing spinel. Leoville 3536-1 (Fig. 2) is devoid of alkali- and halogen-bearing phases and is representative of the primary progenitors of the heavily altered Allende examples [9]; it consists of melilite, spinel, anorthite, and aluminous diopside. These 3 CAIs therefore permit the separate isotopic analysis of primary vs. secondary phases in fine-grained Group II CAIs.

Analytical techniques: Mg isotopes were measured

with a GV Instruments IsoProbe multicollector ICPMS instrument and a New Wave UP193HE excimer laser ablation system at The Field Museum, Chicago. The mass spectrometer was run with a slight positive voltage applied to the extraction lens to minimize Mg background intensities to $< 5 \times 10^{-15}$ A. Individual measurements consist of twenty integration cycles, each of 7 sec duration. The laser spot size was 100 μm , with a repeat rate of 4 Hz and a laser energy density of roughly 2 J cm^{-2} . Signal intensities for ^{24}Mg ranged from 0.6 to 3.0×10^{-11} A. All measurements employed sample-standard bracketing, using isotopically well-characterized synthetic glasses from evaporation experiments having CAI-like compositions (e.g. [10]). Standard glass compositions were chosen that approached the composition of the unknown analyzed phase assemblage. Based on the analyses of these glasses, external reproducibilities (2σ) for Mg isotopic measurements by LA-ICPMS at the Field Museum are $\pm 0.25\%$ for $\delta^{25}\text{Mg}$, $\pm 0.45\%$ for $\delta^{26}\text{Mg}$ and $\pm 0.20\%$ for $\Delta^{26}\text{Mg}$. Internal precisions of individual measurements of unknowns typically are larger, ± 0.3 to 1.3% for $\Delta^{26}\text{Mg}$, because it was not possible to make repeat measurements of the same spot. Our Mg isotopic analyses of terrestrial mineral standards of diopside, spinel and gehlenitic melilite showed no resolvable excesses or deficits in $\Delta^{26}\text{Mg}$ that would indicate that the reported CAI $\Delta^{26}\text{Mg}$ values were affected by matrix effects.

The 100 μm spot size is larger than individual crystals in the CAIs, although many analysis spots encompass $> 40\%$ of a single phase and in some cases as much as 80%. The modal mineralogy of every spot was calculated using image analysis and, independently, least squares fitting of spot bulk composition (obtained by e.d.s. X-ray analysis) with mineral compositions.

Results: The Mg-isotopic data are shown graphically in Fig. 3. All phases in Leoville 3536-1 define an undisturbed correlation line between $^{26}\text{Mg}/^{24}\text{Mg}$ vs. $^{27}\text{Al}/^{24}\text{Mg}$ yielding $(^{26}\text{Al}/^{27}\text{Al})_0 \sim (5.24 \pm 0.86) \times 10^{-5}$. Hibonite-rich spots in Allende 3529-40 (40–60% hib; $< 6\%$ secondary phases) define a line with slope $(^{26}\text{Al}/^{27}\text{Al})_0 \sim (4.78 \pm 0.72) \times 10^{-5}$, indistinguishable within error from the Leoville data. The nepheline- and sodalite-rich regions in Allende 3529-43 define a good correlation between $^{26}\text{Mg}/^{24}\text{Mg}$ and $^{27}\text{Al}/^{24}\text{Mg}$, corresponding to $(^{26}\text{Al}/^{27}\text{Al})_0 \sim (3.33 \pm 0.63) \times 10^{-5}$; secondary minerals in Allende 3529-40 scatter greatly and do not

yield a meaningful correlation.

Discussion: The interpretation that the supra-canonical $(^{26}\text{Al}/^{27}\text{Al})_0$ reported by [2-4] reflects the time of nebular fractionation and condensation of CAI precursors and not necessarily CAI formation is based in part on the fact that the analyzed CAIs have been thermally processed and, in most if not all cases, melted. Yet high-precision multicollector SIMS analyses of individual CAI phases that arguably have *not* been melted (fluffy type A CAIs from CV meteorites [11]; individual hibonite grains from CM meteorites [12]) consistently yield $(^{26}\text{Al}/^{27}\text{Al})_0 < 6 \times 10^{-5}$, most commonly in the range $(4.5\text{--}5.5) \times 10^{-5}$. The primary phases in the unambiguously “condensate” CAIs studied in this work yield $(^{26}\text{Al}/^{27}\text{Al})_0 \sim 5 \times 10^{-5}$ with no evidence of disturbance. Secondary phases in Allende 3529-43 define a lower value, 3.33×10^{-5} , suggesting that secondary alteration postdated the primary condensation event by ~ 0.4 My. Most importantly, these results highlight the fact that early solar system events related to the elemental fractionation and isotopic closure of the Al-Mg system in CAIs still remain poorly understood. One intriguing

model that reconciles our conclusions with those of *e.g.* [4] is multiple episodes of condensation. The nature and timing of the condensation event that caused the Group II trace element fractionation remains very poorly understood even 30 years after the discovery of the Group II pattern. Just as multiple heating and melting events are now commonly accepted in the history of chondrules and CAIs, perhaps multiple condensation events occurred as well.

References: [1] MacPherson G. J. et al. (1995) *MAPS* **30**, 365–386; [2] Galy A. et al. (2004) *LPSC XXXV* #1790; [3] Young E. D. et al. (2005) *Science* **308**, 223–227; [4] Thrane K. et al. (2006) *Astrophys. J.* **646**, L159–L162; [5] Boynton W.V. (1975) *GCA* **39**, 569–584 [6] Davis A.M. and Grossman L. (1979) *GCA* **43**, 1611–1632; [7] Mason B. and Taylor S.R. (1982) *Smithson. Contrib. Earth Sci.* **25**; [8] Mao X.-Y. et al (1990) *GCA* **54**, 2121–2132; [9] Krot A. N. et al. (2004) *MAPS* **39**, 1517–1553; [10] Janney P.E. et al. (2004) *LPSC XXXV* #2092; [11] Cosarinsky M. et al. (2006) *LPSC XXXVII* #2357; [12] Liu M.-C. et al. (2006) *LPSC XXXVII* #2428.

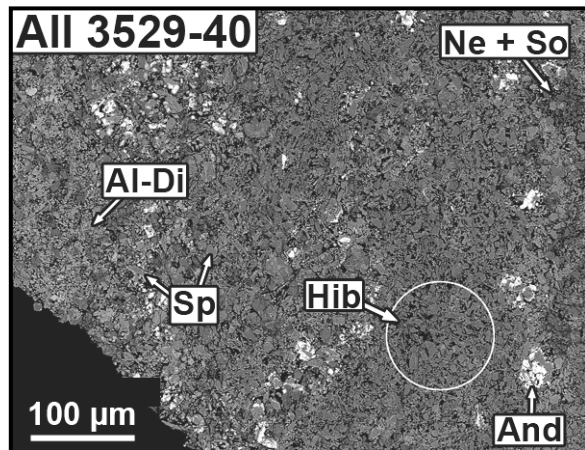


Fig. 1 – B.s.e. image of Allende 3529-40, showing large regions (e.g. circle) that contain 40–60% hibonite. And – andradite; Al-Di – aluminous diopside; Hib – hibonite; Ne + So – nepheline

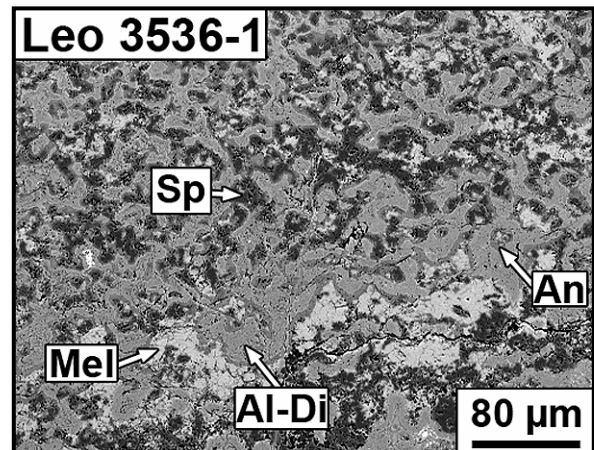


Fig. 2 – B.s.e. image of Leoville 3536-1, showing a complete absence of alkali- and halogen-bearing secondary phases. An – anorthite; Mel – melilite.

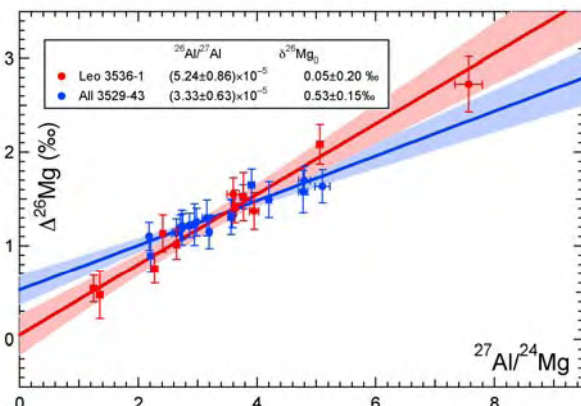
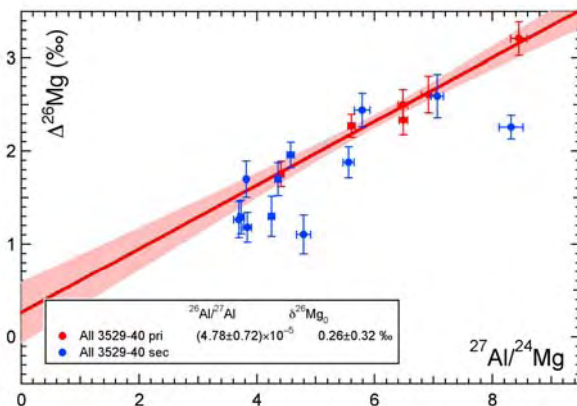


Fig. 3 – Mg isotope data for Allende 3529-40 (L.) and Leoville 3536-1 and Allende 3529-43 (R)